Doubling the resolution of single-molecule localization microscopy with image scanning microscopy

Niels Radmacher[1†], Oleksii Nevskyi[1†], José Ignacio Gallea[1†], Jan Christoph Thiele[3], Ingo Gregor[1], Silvio O. Rizzoli[4], Jörg Enderlein[1,2*]

[1*]Third Institute of Physics – Biophysics, Georg August University, Friedrich-Hund-Platz 1, Göttingen, 37077, Germany.
[2]Cluster of Excellence "Multiscale Bioimaging: from Molecular Machines to Networks of Excitable Cells" (MBExC), Universitätsmedizin Göttingen, Robert-Koch-Str. 40, Göttingen, 37075, Germany.
[3]Department of Chemistry, University of Oxford, South Parks Road, Oxford, OX1 3QZ, UK.
[4]Department of Neuro- and Sensory Physiology, University Medical Center Göttingen, Humboldtallee 23, Göttingen, 37073, Germany.

*Corresponding author(s). E-mail(s): jenderl@gwdg.de;
Contributing authors: niels.radmacher@phys.uni-goettingen.de; oleksii.nevskyi@phys.uni-goettingen.de; ignacio.gallea@phys.uni-goettingen.de; jan.thiele@chem.ox.ac.uk; i.gregor@physik3.gwdg.de; srizzol@gwdg.de;
†These authors contributed equally to this work.

Abstract

Single-molecule localization microscopy (SMLM) is a widely used super-resolution microscopy technique, renowned for its simplicity and impressive achievable resolution. It is typically based on a wide-field fluorescence microscope and relies on emitter photoswitching to capture individual snapshots of a sample with sparse distributions of fluorescent labels. These labels can then be precisely identified and localized. Recently, we demonstrated that SMLM can also be realized with

a fast confocal laser-scanning microscope (CLSM), opening the door to fluorescence lifetime SMLM. This technique has found applications in lifetime-based image multiplexing and metal-induced energy transfer SMLM.
In this work, we present an extension of CLSM-based SMLM by incorporating a single-photon detector array into the CLSM. This enables the combination of CLSM-based SMLM with Image Scanning Microscopy (ISM), a powerful technique for doubling the lateral resolution of a laser-scanning confocal microscope. By doing so, we achieve a two-fold improvement in lateral localization accuracy for SMLM in an easy and straightforward manner. Furthermore, we take advantage of the lifetime information provided by our CLSM for colocalizing different targets without any chromatic aberration. This feature becomes particularly crucial when dealing with the few-nanometer resolution achievable with our system. To demonstrate the capabilities of fluorescence lifetime ISM-SMLM (FL-iSMLM), we perform dSTORM and DNA-PAINT experiments on fluorescently labeled cells, showcasing the resolution-doubling and fluorescence lifetime multiplexing of our system.
Finally, we have developed an open-source software that allows any interested user to easily implement (FL)-iSMLM into an existing CLSM equipped with a fast array detector. This user-friendly approach enables widespread adoption and application of (FL)-iSMLM in various research settings.

Keywords: super-resolution microscopy, single-molecule localization microscopy, image-scanning microscopy, fluorescence lifetime microscopy

1 Introduction

Over the past decades, super-resolution microscopy has become a fundamental tool in bioimaging, finding manifold applications in biophysics and cell biology. One of the most popular and powerful super-resolution modalities is Single-Molecule Localization Microscopy (SMLM). This encompasses techniques like Photoactivated Localization Microscopy (PALM) [1], (direct) Stochastic Optical Reconstruction Microscopy (STORM [2] and dSTORM [3]), Point Accumulation for Imaging in Nanoscale Topography (PAINT) [4], and its especially potent variant DNA-PAINT [5]. Nowadays, SMLM can achieve lateral resolutions below one nanometer [6], two orders of magnitude better than the diffraction limit of classical optical microscopy.

Typically, SMLM is based on a wide-field microscope, enabling the detection and localization of single molecules over a large field of view. Recently, we developed a variant of SMLM based on a rapid Confocal Laser-Scanning Microscope (CLSM), which combines the super-resolution of SMLM with FLuorescence Lifetime Imaging (FLIM) [7**?**]. The additional fluorescence lifetime information not only allows for target multiplexing in imaging but also facilitates the combination of SMLM with Metal-Induced Energy Transfer (MIET) imaging [9–11]. MIET uses the modulation of fluorescence lifetime by a nearby metal layer to achieve nanometer resolution along the optical axis. By merging FL-SMLM with MIET, we achieved an isotropic single-molecule localization with a few nanometers localization accuracy along all three dimensions.

In this paper, we synergize CLSM-based fluorescence-lifetime SMLM (FL-SMLM) with another cutting-edge high-resolution technique known as Image Scanning Microscopy (ISM) [12, 13]. ISM employs a blend of focused laser excitation and wide-field imaging, accomplished by augmenting a CLSM with an array detector. This setup enables the capture of a miniature image of the illuminated sample at each scanning position of the CLSM. Through meticulous image reconstruction [14–16], ISM effectively doubles the lateral resolution and quadruples image contrast by reducing the effective point spread function by a factor of two.

The resolution enhancement accomplished by ISM is akin to that achieved by Structured Illumination Microscopy (SIM) [17], which also employs non-uniform structured illumination and wide-field detection to double the lateral resolution. In the realm of SMLM, ISM promptly enhances the accuracy of single-molecule localizations, thus significantly elevating the ultimate SMLM resolution. From a perspective rooted in physical optics, this mirrors the twofold increase in localization accuracy achieved through patterned illumination techniques like SIMPLE [18, 19], SIMFLUX [20], as well as others [21, 22]. However, ISM offers a substantial reduction in experimental complexity. Instead of illuminating the sample with variously positioned and oriented excitation patterns, ISM merely requires the augmentation of a CLSM with a compact array detector and the acquisition of scan images of the sample in the standard CLSM operational mode.

Many published variants of ISM employ rapid cameras for recording the fluorescence signal, which lack the capability for performing fluorescence lifetime imaging (FLIM) [23, 24]. However, Tenne et al. pioneered the integration of several Single-Photon Avalanche Detector (SPAD) detectors and fast multichannel Time-Correlated Single Photon Counting (TCSPC) electronics, thus introducing fluorescence lifetime ISM [25, 26]. Recent developments in SPAD array technology have further extended the possibilities of combining ISM with FLIM [27–30].

In this work, we have incorporated a SPAD array detector along with fast TCSPC electronics into our CLSM system to enable fluorescence-lifetime image-scanning SMLM (FL-iSMLM). We rigorously validate and calibrate our FL-iSMLM system using fluorescent point-spread function beads. Subsequently, we demonstrate its capabilities by imaging the intricate microtubule lattice within fixed COS-7 cells. Furthermore, we present fluorescence lifetime-based two-target FL-iSMLM imaging of actin and tubulin. The achieved lateral resolution, approximately ∼5 nm, underscores the significance of FL-iSMLM, as it ensures the complete elimination of chromatic aberration.

Finally, we illustrate a biologically meaningful application by simultaneously imaging Homer1 and Bassoon proteins in the synaptic cleft of neurons using DNA-PAINT-based FL-iSMLM.

2 Results

2.1 ISM calibration

ISM calibration and Single-Molecule Localization Microscopy (SMLM) measurements were conducted using our custom-made time-resolved laser scanning microscope, as

depicted in Fig. 1(a) for detailed specifications. This microscope is equipped with a high-speed galvo scanner capable of capturing scan images at high speeds.

For excitation, we employed either a 640 nm or 561 nm pulsed laser. This setup, combined with our picosecond multichannel event timer, enabled us to utilize Time-Correlated Single Photon Counting (TCSPC) for precise fluorescence lifetime measurements.

The analysis of the acquired data was carried out using our in-house software, TrackNTrace [31], specifically amended for this purpose.

To compute the correct shift vectors for ISM pixel reassignment (similar to the phase correlation approach used in [27]) and validate the resolution improvement, we conducted scans of sub-diffraction beads under the same conditions as used for the ISM dSTORM and DNA-PAINT measurements. Fig. 1(b) illustrates the calculated shift vectors.

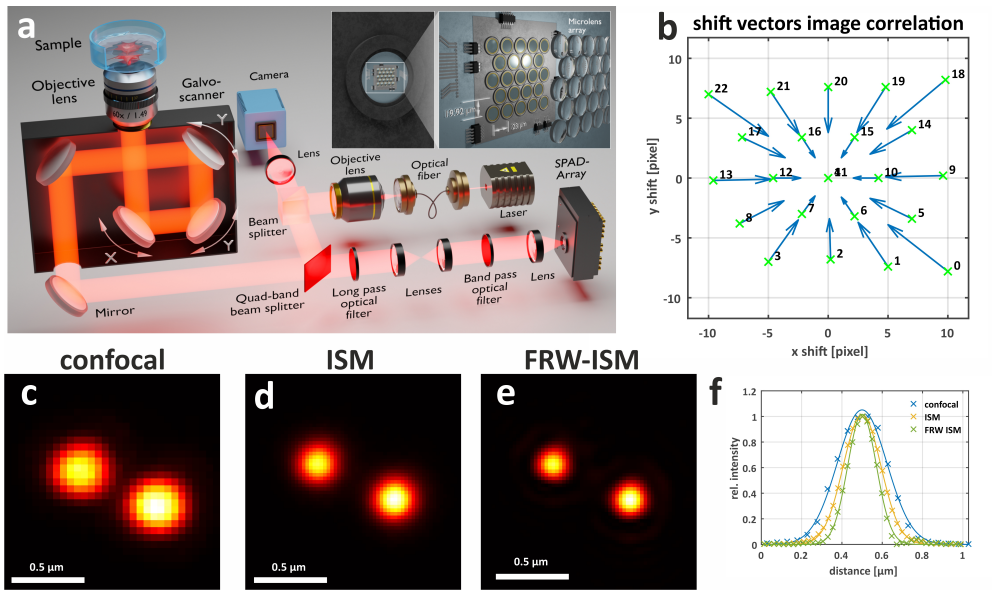

Fig. 1 (a) Schematic of the FL-iSMLM setup. The inset depicts the arrangement of the 23 individual SPAD pixels and a micro lens array, which increases the fill factor of the detector up to 82%. (b) Shift vectors for ISM pixel reassignment. Green crosses represent pixel positions relative to the optical axis, and blue arrows indicate the ISM shift vectors. Pixel 5 does not have a shift vector because it is discarded due to its significantly increased dark-count rate (1.5 kcps at 7°C). The average dark-count rate across the other 22 pixels is 35 cps at 7°C. (c, d, and e) Images of sub-diffraction beads (Gatta Beads red, 23 nm, labeled with Atto 647N, GATTAQUANT GmbH). (c) Confocal image obtained by summing the signal over all detector pixels. (d) Photon detection positions adjusted according to ISM pixel reassignment. (e) Fourier-reweighted ISM image. (f) Intensity trace across one bead. The calculated 2σ resolution is 246±4 nm, 186±1 nm, and 142.2±1.7 nm for confocal, ISM, and Fourier-reweighted ISM, respectively.

To determine these vectors, we employed image correlation to ascertain the shift of each individual detector pixel relative to the optical axis. Prior to this, the SPAD-Array

was aligned so that the central pixel of the hexagonal pattern (as seen in Fig. 1(a)) coincided with the optical axis. Subsequently, the scan images captured by the various individual pixels of the SPAD array were correlated with the scan image recorded by the central pixel. The position of the maximum in the resulting correlation map provided the necessary shift for the scan image recorded by a specific pixel in relation to the central pixel. These reassignment vectors are illustrated in Fig. 1(b), where the green crosses represent the actual positions of the 23 pixels, and the arrows indicate the direction and magnitude of the shift. The units are given in the number of scan steps (in our case, 50 nm).

Fig.s 1(c)-(e) demonstrate the resolution enhancement of ISM and Fourier-reweighted ISM compared to Confocal Laser Scanning Microscopy (CLSM). To quantify this improvement, we plotted intensity profiles across one of the beads and calculated its 2σ width, as shown in Fig. 1(f). The confocal image, obtained by summing photons from all detector pixels, yielded a 2σ value of 248 ± 4 nm. With ISM reassignment, this value decreased to 186 ± 1 nm. Further Fourier reweighting, as detailed in [13], improved this value to 142.2 ± 1.7 nm, resulting in a total improvement by a factor of 1.73 compared to CLSM.

2.2 Super-resolution imaging with iSMLM

For the FL-iSMLM measurements, we selected a region of interest measuring 5 µm × 5 µm, capturing images at a frame rate of 27.9 Hz. Approximately $5 \cdot 10^4$ to $7.5 \cdot 10^4$ images were recorded to ensure a sufficient number of single molecule blinking events.

To optimize single-molecule localization, we applied frame binning by combining 10 frames before conducting further image analysis. This approach helps prevent Point Spread Function (PSF) distortions arising from photoswitching during scanning, ensuring an even distribution of the photon budget across all scan positions.

For localization and lifetime analysis, we employed the open-source tool Track-NTrace [32], which was extended to include ISM pixel reassignment, adjusting the position of each recorded photon event during the measurement [31]. Subsequently, Fourier reweighting was applied to the resulting ISM images, following the method described in Ref. [13] (also detailed in the Methods section below).

The resulting images were then used for single molecule localization, ultimately yielding the final super-resolved image. To determine the lifetime of each localized single molecule, we collected all photons from the event and performed tail-fitting using a mono-exponential decay function on the corresponding Time-Correlated Single Photon Counting (TCSPC) histogram (as further outlined in the Methods section below). Notably, photons from molecules appearing in subsequent frames were combined into a single event.

To showcase the localization improvement achieved by iSMLM, we immunolabeled α-tubulin in COS-7 cells using Alexa 647-conjugated antibodies. The on-off photoswitching of the fluorophores was initiated using a PBS buffer containing cysteamine. Fine-tuning the blinking behavior, and consequently the number of photons per localization event, was achieved by varying the composition of this photoswitching buffer.

For the dSTORM measurement, we initially selected a suitable region of interest where most of the microtubules lay in the same plane, as depicted in the zoom-in I of Fig. 2(a). Subsequently, we defined a 5 µm×5 µm region of interest, as shown in zoom-in II. The final SMLM images are presented in Fig. 2(b)-(d), and these images were reconstructed using three different approaches: dSTORM without ISM photon reassignment, with ISM photon reassignment, and with photon reassignment plus Fourier reweighting, respectively.

To enhance the fidelity of the image reconstruction and eliminate localizations that could result from single molecule mis-identifications, we only considered events with more than 100 photons and single-molecule image widths smaller than 500 nm. The width of a single molecule image was defined as the 2σ size of a fitted circularly symmetric 2D Gaussian intensity distribution. Additionally, molecule images that occurred in several subsequent frames were combined into a single event.

The average σ value of single molecule images (the average σ values of Gaussian fits) for the single-molecule localizations in Fig. 2(b) was 160 nm, as indicated in panel (f), which falls within the range of the measured Point Spread Function (PSF) determined from the bead calibration measurements. The median localization precision of dSTORM was estimated at 9.5 nm, as calculated using a modified Mortensen's equation [33]. This value improved to 6.5 nm after ISM photon reassignment, with a corresponding σ value of 115 nm. The reconstructed image, Fig. 2(c), also revealed finer details, particularly noticeable in regions where microtubules overlap. Finally, after Fourier reweighting, the localization precision further increased to 5.3 nm.

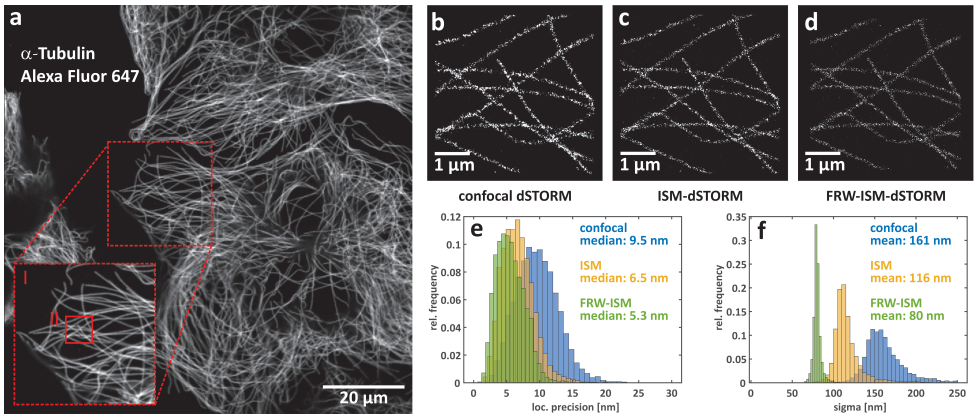

Fig. 2 Single labeling iSMLM dSTORM results. (a) Overview of a COS-7 cell where α-tubulin was labeled with Alexa 647. Zoom I depicts a more detailed field of view. Zoom II is the actual 5 µm × 5 µm region used for dSTORM analysis. (b-d) Confocal, ISM and Fourier-reweighted ISM dSTORM reconstruction from $5 \cdot 10^4$ images with 10 frame binning. (e) Localization precision for confocal, ISM and Fourier-reweighted ISM dSTORM of α-tubulin. (f) Histograms of fitted σ values of localization events for confocal, ISM and Fourier-reweighted ISM dSTORM.

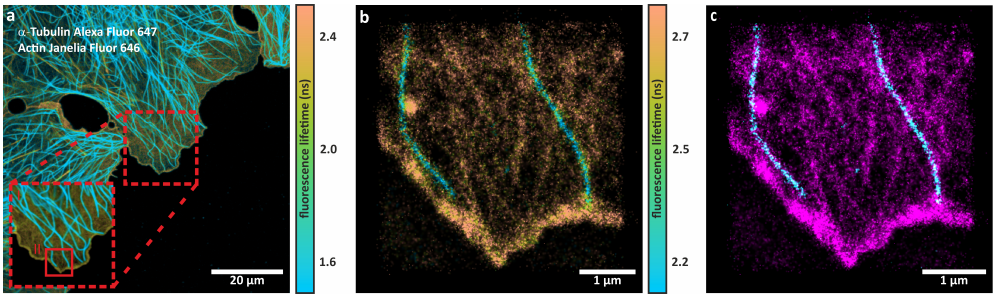

Fig. 3 dSTORM based FL-iSMLM multiplexing. (a) Overview of a COS-7 cell where α-tubulin was labeled with Alexa 647 and actin with phalloidin-Janelia Fluor 646. Zoom II shows the actual 5 µm × 5 µm region used for dSTORM analysis. (b) Super-resolved FL-iSMLM dSTORM reconstruction from $6.5 \cdot 10^4$ images with 10 frame binning. (c) False color super-resolved image based on fluorescence lifetime data. The two lifetime components were separated using lifetime pattern matching. Localization events identified as Alexa 647 are colored cyan, and localization events identified as Janelia Fluor 646 are colored magenta. The identification accuracy, as estimated from the overlap of the fluorescence lifetime histograms of Alexa 647 and Janelia Fluor 646, was better than 99%.

2.3 FL-iSMLM multiplexing

The availability of lifetime information in FL-iSMLM allows for image multiplexing, enabling the simultaneous imaging of different targets based on the distinct fluorescence lifetimes of the applied labels. To demonstrate this capability, we labeled COS-7 cells with α-tubulin and F-actin using antibody-conjugated Alexa 647 and phalloidin-Janelia Fluor 646, respectively. Both fluorophores exhibited comparable on-off photoswitching behavior and similar quantum yields under the same buffer conditions, making them an ideal combination for lifetime-multiplexed FL-iSMLM.

In Fig. 3(a), we present a confocal image of one of these cells, where color represents the average fluorescence lifetime, calculated as the mean photon arrival time. The square denotes the region of interest chosen for dSTORM measurement. In this analysis, we recorded $6.5 \cdot 10^4$ images at a frame rate of 27.2 Hz, totaling just under 40 minutes of acquisition time. The resulting data underwent analysis using our open-source software, TrackNTrace, with the newly incorporated ISM plugin [31].

For each localization event, we determined the fluorescence lifetime by collating all photons associated with the event and subsequently performing a mono-exponential tail-fitting using a Maximum-Likelihood Estimator (MLE). Tail-fitting involves removing the excitation peak from the TCSPC curve and retaining only photons arriving later than 0.3 ns after the TCSPC curve's peak. The resulting FL-iSMLM super-resolution image is displayed in Fig. 3(b), revealing a distinct separation of structures based on lifetime: The short lifetime events at ∼1.7 ns correspond to Alexa 647-labeled α-tubulin, while the long lifetime components at ∼2.8 ns correspond to actin filaments. We also employed a pattern-matching-based classification to distinguish these two structures. This involved first determining the decay patterns for only Alexa 647-labeled α-tubulin and phalloidin-Janelia Fluor 646-labeled actin using samples with only one respective labeling. We then utilized these patterns to separate the single-molecule events in the doubly-labeled samples [34].

The resulting false-color image is presented in Fig. 3(c), with Alexa 647 localizations represented in cyan and Janelia Fluor 646 localizations in magenta. In this context, localizations with a probability of less than 99% of corresponding to their respective decay patterns were systematically excluded from the reconstruction. Notably, the FL-iSMLM image unveils intricate actin filament structures that were previously indiscernible in the confocal image.

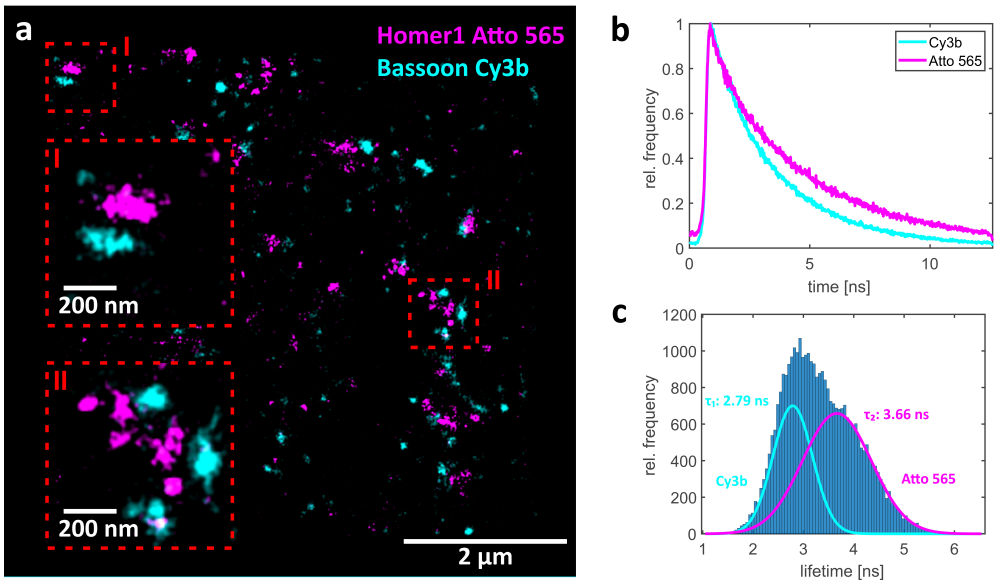

Fig. 4 DNA-PAINT-based FL-iSMLM multiplexing. (a) Super-resolved Fourier-reweighted iSMLM image of Homer1 labeled with Atto 565 (magenta) and Bassoon labeled with Cy3b (cyan). Targets were separated by using fluorescence-lifetime pattern-matching classification. (b) Fluorescence lifetime decay curves for pure Cy3b and Atto 565 samples, respectively. (c) Fluorescence lifetime histogram obtained from single molecule localizations in (a), fitted with two Gaussian distributions.

We conducted a repeat dSTORM measurement at the center of another COS-7 cell, which exhibited a comparable density of actin and tubulin. An overview of this cell is presented in Fig. S1(a), where color is used to represent fluorescence lifetime. In Fig. S1(b), we showcase a super-resolved fluorescence-lifetime image obtained through FL-iSMLM within the region enclosed by the red square. The corresponding lifetime histogram reveals two distinct and well-separated peaks, both of which have been fitted with Gaussian distributions.

To generate the dual-color image featured in Fig. S1(d), we once again employed a pattern-matching classifier. This classifier utilized the same pre-established decay patterns as those applied in Fig. 3.

To showcase the capabilities of FL-iSMLM on a biologically more relevant sample, we employed DNA-PAINT [35, 36] to visualize pre- and postsynaptic scaffolds, Bassoon and Homer1, within cultured hippocampal neurons. These proteins are situated

across the synaptic cleft and are known to form domains that organize into relatively flat structures: the presynaptic active zone and the postsynaptic density (PSD), respectively. To label these proteins, we used specific antibodies conjugated with DNA target strands. Bassoon was imaged using DNA imager strands labeled with Cy3b, while Homer1 was imaged using DNA imager strands labeled with Atto 565.

In Fig. 4(a), we present FL-iSMLM reconstructions of a 7 µm × 7 µm field of view in a hippocampal cell. Confocal scan images were acquired with 70 nm scan steps and the same dwell time as in previous measurements. We recorded a total of 10^5 images over an acquisition time of just over one hour. To account for the DNA-PAINT binding rates, we increased frame binning from 10 to 20 frames. Image reconstruction was once again performed using TrackNTrace, which was amended with ISM capabilities [31]. The localization events were classified using fluorescence lifetime pattern matching, following the same methodology as previously described.

For this analysis, reference lifetime patterns were derived from DNA-PAINT fluorescence lifetime images of pure samples in which either Bassoon or Homer1 was exclusively labeled. The resulting TCSPC histograms are displayed in Fig. 4(b). Notably, we observed a subtle lifetime difference of only 0.9 ns between Cy3B and Atto 565 labeled proteins, as depicted in Fig. 4(c). This minor difference necessitated the use of pattern matching for accurate lifetime classification of single molecule localization events. In the reconstructed images, localization events attributed to the decay pattern of Cy3B, with a probability exceeding 99%, are depicted in cyan, whereas those associated with Atto 565, with an equivalent confidence level, are indicated in magenta. All other events have been excluded from this reconstruction.

Our FL-iSMLM DNA-PAINT images vividly depict the distribution of two proteins as neighboring pairs of densely packed molecular structures, with a clear separation by the synaptic cleft. This observation is consistent with findings reported in the literature [37]. The average distance between Bassoon and Homer1 across the synaptic cleft, determined by measuring the separation between the peak positions of their respective localizations (as exemplified in Fig. S2), was measured at ∼150 nm. This measurement aligns closely with previously published values [37, 38].

3 Methods

3.1 FL-iSMLM setup

All measurements in this study were conducted using a custom-made ISM setup, as illustrated in Fig. 1(a). For excitation, we employed a 640 nm pulsed laser diode with a 40 MHz repetition rate and a pulse width of ≤90 ps (PDL 800-B driver with LDH-D-C-640 diode, PicoQuant) and a 561 nm supercontinuum white light laser with a 80 MHz repetition rate (Fianium WhiteLaser SC450, NKT Photonics). The laser beam was coupled into a single-mode optical fiber (PMC-460Si-3.0-NA012-3APC-150-P, Schäfter + Kirchhoff) using a fiber coupler (60SMS-1-4-RGBV-11-47, Schäfter + Kirchhoff).

After the fiber, the laser light was collimated using an air objective (UPlanSApo 10x/0.40 NA, Olympus) and passed through a clean-up filter (MaxDiode 640/8, Semrock or BrightLine 563/9, Semrock) before being directed to the microscope through an ultra-flat quad-band dichroic mirror (ZT 405/488/561/640 RPC, Semrock). Laser

scanning was achieved using a three-galvo mirror scan system (FLIMbee, PicoQuant) with an integrated 2x magnification telescope. The laser light was focused onto the sample using a high numerical-aperture oil immersion objective (UApo N 100×/1.49 NA oil, Olympus).

Samples were mounted on a manual xy stage (Olympus) equipped with a z-piezo stage (Nano ZL100, Mad City Labs) for precise focus control. The same objective was used for collecting the fluorescence light (epi-fluorescence configuration), which was then de-scanned in the FLIMbee system. After passing through the quad-band beam splitter, the emission light was focused through a pinhole (100-µm P100S, Thorlabs) using an achromatic lens (TTL180-A, Thorlabs). The pinhole was solely used for optical component alignment and was removed during the ISM and iSMLM measurements.

To eliminate back-reflected and scattered light, a long-pass filter (635 LP or 561 LP Edge Basic, Semrock) was placed in front of two achromatic lenses (AC245-100-A-ML and AC254-075-A-ML, Thorlabs), which relayed the emission light onto a single-photon avalanche diode array (SPAD array) detector (SPAD23, PI Imaging Technology). The SPAD array consists of 23 individual SPADs arranged in a hexagonal pattern, with a pixel-to-pixel distance of 23 µm. This array is equipped with a matching microlens array, which boosts its fill factor beyond 80%, leading to a total photon detection efficiency of 23.5% at 700 nm and 35% at 600 nm. A band-pass filter (BrightLine HC 708/75, Semrock or BrightLine HC 617/73, Semrock) was employed to further suppress scattered light.

The output signals from the 23 pixels were independently recorded using a TCSPC module (Multi Harp 160, PicoQuant), controlled by the SymPhoTime 64 software (PicoQuant). The software also controlled the galvo and piezo scanners. Samples were scanned with step sizes of 50 nm to 70 nm, with a dwell time of 2.5 µs and a temporal resolution for photon-detection event timing of 20 ps.

3.2 Cell culture and immunostaining

COS-7 cell line culture. A COS-7 African Green Monkey fibroblast-like cell line was cultured at 37°C with 5% CO_2 in T25-culture flasks, using Dulbecco's Modified Eagle Medium (DMEM) supplemented with 10% FBS (Sigma-Aldrich, F7524) and 100 U/ml penicillin + 0.1 mg/ml streptomycin (Sigma P4333). One day before use, cells were seeded onto 35 mm glass bottom Ibidi dishes (µ-Dish 35 mm high, 81158) at a concentration of 10^5 cells/dish, and cultivated overnight.

Hippocampal cultured neurons. Experimental procedures involving animals (Wistar rats, P0 to P1) were conducted in accordance with the guidelines of the local regulatory authority, the Lower Saxony State Office for Consumer Protection and Food Safety (Niedersächsisches Landesamt für Verbraucherschutz und Lebensmittelsicherheit), under license Tötungsversuch T09/08. Briefly, hippocampi were dissected from rat brains, followed by washing using Hank's Balanced Salt Solution (HBSS, 14175053, Invitrogen, Waltham, MA, USA). Then, hippocampi were gently agitated in a digestion solution, which included 15 U/ml papain (LS003126, Worthington, Lakewood, USA), alongside with 1 mM $CaCl_2$, 0.5 mM EDTA, and 0.5 mg/ml L-cysteine (30090, Merck), all dissolved in DMEM. This enzymatic digestion was performed for 1 h at

37°C, before inactivation with a buffer solution containing 10% FCS and 5 mg/ml bovine serum albumin (BSA, A1391, Applichem, Darmstadt, Germany) in DMEM. After 15 minutes, this inactivation solution was replaced with growth medium containing 10% horse serum (S900-500, VWR International GmbH, Darmstadt, Germany), 1.8 mM glutamine, and 0.6 mg/ml glucose in MEM (51200046, ThermoFisher Scientific), which was utilized for the subsequent iterative washes of the hippocampal tissue. Afterwards, the neurons were isolated by trituration, a method that uses a glass pipette for mechanical disruption, then separated by centrifugation at 800 rpm (8 minutes), and re-suspended in the same medium. The neurons were then seeded onto poly-L-lysine-coated coverslips and allowed to adhere for several hours before being transferred to Neurobasal™-A medium (10888022, ThermoFisher Scientific) with 0.2% B27 supplement (17504-044, ThermoFisher Scientific) and 2 mM GlutaMAX (35050-038, ThermoFisher Scientific). Finally, neurons were maintained in a humidified incubator (5% CO_2, 37°C) for at least 14 days before use.

Immunostaining of cytoskeletal proteins. For microtubule and actin immunolabeling, COS-7 cells were washed with pre-warmed (37°C) PBS, and permeabilized for 2 min with 0.3% glutaraldehyde (GA) + 0.25% Triton X-100 (Sigma-Aldrich, 340855 and Thermo Fisher, 28314) in pre-warmed (37°C) cytoskeleton buffer (CB) at pH 6.1, consisting of 10 mM MES (Sigma-Aldrich, M8250), 150 mM NaCl (Sigma-Aldrich, 55886), 5 mM EGTA (Sigma-Aldrich, 03777), 5 mM glucose (Sigma-Aldrich, G7021), and 5 mM $MgCl_2$ (Sigma-Aldrich, M9272). After permeabilization, cells were fixed with a pre-warmed (37°C) solution of 2% GA in CB for 10 min. After fixation, cells were washed twice with PBS and reduced with 0.1% sodium borohydride (Sigma-Aldrich, 71320) in PBS for 7 min. Cells were again washed three times with PBS before blocking with 5% BSA (Roth, 3737.3) in PBS for 1 h. Subsequently, cells were incubated with 10 ng/µl anti-alpha tubulin antibody (DM1A) (Abcam, ab264493) in a blocking buffer for 1 h. After primary antibody incubation, cells were washed thrice with 0.1% Tween 20 (Thermo Fisher, 28320) in PBS for 15 min. After washing, cells were incubated in a blocking buffer with 20 ng/µl of commercial secondary antibody goat anti-mouse IgG H&L (Alexa Fluor 647) (abcam, ab150115) for 45 min. After secondary antibody incubation, cells were again washed three times with 0.1% Tween 20 in PBS for 15 min. After washing, a post-fix with 4% formaldehyde (Sigma-Aldrich, F8775) in PBS for 10 min was performed, followed by three additional washing steps with PBS.

If actin was also fluorescently labeled, a final incubation step with a solution of 500 nM phalloidin-Janelia Fluor 646 in PBS for one hour was performed prior to imaging. This was followed by three washing cycles with PBS.

Immunostaining of synaptic proteins. Neurons were fixed with 4% PFA and 0.2% GA in PBS for 30 min before being quenched with a 0.1% sodium borohydride solution for 9 min. These cells were then exposed to a blocking/permeabilizing solution containing 5% BSA and 0.1% Triton X-100 in PBS for 30 min. Primary antibodies against Homer1 (160003, Synaptic Systems) and Bassoon (ADI-VAM-PS003-F, Enzo, New York, USA) were diluted in 5% BSA in PBS and applied to the coverslips for 60 min. Then, samples were washed three times with a solution of 0.1% Tween in

PBS, followed by immersing the coverslips for 45 minutes in a diluted solution of secondary single domain antibodies with DNA strands (FluoTag®-XM-QC Anti-Mouse IgG kappa light chain + FAST docking site F1 and FluoTag®-XM-QC Anti-Rabbit IgG + FAST docking site F2) in 5% BSA in PBS. Samples were then washed three times with 0.1% Tween in PBS before imaging.

3.3 SMLM imaging

For confocal dSTORM imaging with only Alexa 647 dye, a switching buffer consisting of 50 mM cysteamine in PBS at pH 7.4 was used. For dual-color imaging with both Alexa 647 and Janelia Fluor 646 dyes, an enzymatic oxygen scavenging buffer (glucose oxidase 0.5 mg/ml, catalase 40 g/ml, glucose 10% w/v in PBS at pH 7.4) with the addition of 50 mM cysteamine was used. For DNA-PAINT imaging of proteins in hippocampal neurons, the commercial imaging buffer MASSIVE-SDAB-FAST 2-PLEX kit (Massive Photonics) containing 770 pM Cy3b-labeled imager F1 and 500 pM Atto 565-labeled imager F2 was used.

3.4 Data analysis

FL-iSMLM measurements were analyzed using an extended version of the TrackNTrace software package [31]. To generate images from the raw scan data, we combined 10 scans into a single frame. In the localization process, we utilized the "Cross-Correlation" detection plugin with default parameters and the "TNT Fitter" refinement plugin, employing pixel-integrated Gaussian Maximum Likelihood Estimation (MLE) fitting.

Localizations found in adjacent frames with a separation of less than 100 nm were considered to originate from the same molecule. Their positions were subsequently refitted using the photon detection events from all relevant frames. For the purpose of lifetime fitting, we constructed a Time-Correlated Single Photon Counting (TCSPC) histogram for each localized molecule by collecting all photons within a circle with a radius of less than 2 times the standard deviation (σ_{PSF}) from the molecule's center position. These TCSPC histograms were then fitted with a mono-exponential decay function using Maximum Likelihood Estimation (MLE) to determine the lifetime, as also detailed in Ref. [34].

In the context of iSMLM, photon positions were reassigned utilizing ISM shift vectors obtained through the imaging of PSF beads with a diameter of 23 nm, as discussed in the preceding Results section. This reassignment was performed prior to frame binning and event localization. Fourier reweighting was applied to the combined frame data following the algorithm detailed in Ref. [13]. The necessary Optical Transfer Function (OTF) was computed through the Fourier transformation of the detection PSF from our microscope, which had been parameterized using the same bead image employed for shift vector calibration. For the normalization parameter ϵ (see [13]), which averts the amplification of image noise at high frequencies in Fourier space, we selected a value of 0.04 of the maximum of the OTF. Both photon reassignment and Fourier reweighting have been incorporated into the extended version of TrackNTrace [31].

4 Discussion

In this study, we introduced an enhanced version of Single-Molecule Localization Microscopy (SMLM) by integrating Image Scanning Microscopy (ISM) with SMLM. This integration significantly improved resolution and expanded the capabilities of our imaging setup. To achieve this advancement, we extended an existing Confocal Laser Scanning Microscopy (CLSM) system by incorporating a Single-Photon Avalanche Diode (SPAD) array detector. Combined with high-speed Time-Correlated Single Photon Counting (TCSPC) electronics, this upgraded CLSM not only increased the precision of molecular localization but also allowed us to capture the fluorescence lifetimes of individual molecules. This capability enabled us to perform multi-target SMLM without the adverse effects of chromatic aberration, which is particularly critical when aiming for localization precision below 10 nm.

Utilizing the unique lifetime multiplexing feature of our Fluorescence Lifetime-integrated SMLM (FL-iSMLM), we simultaneously visualized two crucial components of the cytoskeleton: microtubules and actin filaments. Even in scenarios with substantial differences in target protein concentrations, our highly efficient pattern matching classification reliably distinguished and separated both structures.

Furthermore, we used DNA-PAINT-based FL-iSMLM to provide nanometer-scale precision in depicting the spatial arrangement of synaptic scaffolds Homer1 and Bassoon. These proteins form closely apposed structures on opposite sides of the synapse, and our technique allowed us to visualize their arrangement with excellent precision.

In our ongoing effort to facilitate broader adoption of this advanced imaging method, we have expanded the capabilities of our publicly available single-molecule tracking and localization software, TrackNTrace [32]. We introduced a novel FL-ISM-plugin that [31], in combination with the SPAD-array detector, simplifies and promotes the widespread implementation of FL-iSMLM.

Supplementary information. Two supplementary figures are provided in the supplementary information file, as referenced in the main text.

Acknowledgments. We thank Alexey Chizhik for providing us with the illustration of our ISM microscope setup.

Declarations

- Funding: NR, JE and SOR acknowledge financial support by the Bundesministerium für Bildung und Forschung (BMBF) of Germany via project NG-FLIM (project number 13N15327 and 13N15328). JIG acknowledges financial support from the European Union's Horizon 2021 research and innovation programme under the Marie Skłodowska-Curie Grant Agreement no. 101062508 (project name: SOAD-OPP). JE and JIG acknowledge financial support by the DFG through Germany's Excellence Strategy EXC 2067/1-390729940. JE and ON thank the European Research Council (ERC) for financial support via project "smMIET" (grant agreement no. 884488) under the European Union's Horizon 2020 research and innovation program.
- Conflict of interest: The authors declare no conflict of interest.
- Availability of data and materials: https://gitlab.gwdg.de/igregor/single-molecule-localization-microscopy-with-image-scanning-microscopy.git
- Code availability: https://gitlab.gwdg.de/igregor/single-molecule-localization-microscopy-with-image-scanning-microscopy.git
- Contributions of authors: NR and ON built the setup, performed the microscopic imaging, and analyzed the data. JIG prepared the samples and performed the microscopic imaging. JCT helped with the implementation of the ISM plugin for the analysis software. IG helped with setup and experiments. JE conceived the idea, worked out the theoretical framework and helped with data analysis. NR, ON, JIG, SOR and JE wrote the manuscript.

References

[1] Betzig, E., Patterson, G.H., Sougrat, R., Lindwasser, O.W., Olenych, S., Bonifacino, J.S., Davidson, M.W., Lippincott-Schwartz, J., Hess, H.F.: Imaging intracellular fluorescent proteins at nanometer resolution. Science **313**(5793), 1642–1645 (2006)

[2] Huang, B., Wang, W., Bates, M., Zhuang, X.: Three-dimensional super-resolution imaging by stochastic optical reconstruction microscopy. Science **319**(5864), 810–813 (2008)

[3] Heilemann, M., Linde, S., Schüttpelz, M., Kasper, R., Seefeldt, B., Mukherjee, A., Tinnefeld, P., Sauer, M.: Subdiffraction-resolution fluorescence imaging with conventional fluorescent probes. Angewandte Chemie International Edition **47**(33), 6172–6176 (2008)

[4] Sharonov, A., Hochstrasser, R.M.: Wide-field subdiffraction imaging by accumulated binding of diffusing probes. Proceedings of the National Academy of Sciences **103**(50), 18911–18916 (2006)

[5] Schnitzbauer, J., Strauss, M.T., Schlichthaerle, T., Schueder, F., Jungmann, R.: Super-resolution microscopy with DNA-PAINT. Nature Protocols **12**(6), 1198–1228 (2017)

[6] Reinhardt, S.C., Masullo, L.A., Baudrexel, I., Steen, P.R., Kowalewski, R., Eklund, A.S., Strauss, S., Unterauer, E.M., Schlichthaerle, T., Strauss, M.T., *et al.*: Ångström-resolution fluorescence microscopy. Nature **617**(7962), 711–716 (2023)

[7] Thiele, J.C., Helmerich, D.A., Oleksiievets, N., Tsukanov, R., Butkevich, E., Sauer, M., Nevskyi, O., Enderlein, J.: Confocal fluorescence-lifetime single-molecule localization microscopy. ACS nano **14**(10), 14190–14200 (2020)

[36] Oleksiievets, N., Sargsyan, Y., Thiele, J.C., Mougios, N., Sograte-Idrissi, S., Nevskyi, O., Gregor, I., Opazo, F., Thoms, S., Enderlein, J., *et al.*: Fluorescence lifetime DNA-PAINT for multiplexed super-resolution imaging of cells. Communications Biology **5**(1), 38 (2022)

[9] Chizhik, A.I., Rother, J., Gregor, I., Janshoff, A., Enderlein, J.: Metal-induced energy transfer for live cell nanoscopy. Nature Photonics **8**(2), 124–127 (2014)

[10] Isbaner, S., Karedla, N., Kaminska, I., Ruhlandt, D., Raab, M., Bohlen, J., Chizhik, A., Gregor, I., Tinnefeld, P., Enderlein, J., *et al.*: Axial colocalization of single molecules with nanometer accuracy using metal-induced energy transfer. Nano Letters **18**(4), 2616–2622 (2018)

[11] Thiele, J.C., Jungblut, M., Helmerich, D.A., Tsukanov, R., Chizhik, A., Chizhik, A.I., Schnermann, M.J., Sauer, M., Nevskyi, O., Enderlein, J.: Isotropic three-dimensional dual-color super-resolution microscopy with metal-induced energy transfer. Science Advances **8**(23), 2506 (2022)

[12] Sheppard, C.R.: Super-resolution in confocal imaging. Optik (Stuttgart) **80**(2), 53–54 (1988)

[13] Müller, C.B., Enderlein, J.: Image scanning microscopy. Physical Review Letters **104**(19), 198101 (2010)

[14] Sheppard, C.J., Mehta, S.B., Heintzmann, R.: Superresolution by image scanning microscopy using pixel reassignment. Optics Letters **38**(15), 2889–2892 (2013)

[15] Sheppard, C.J., Castello, M., Tortarolo, G., Vicidomini, G., Diaspro, A.: Image formation in image scanning microscopy, including the case of two-photon excitation. Journal of the Optical Society of America A **34**(8), 1339–1350 (2017)

[16] Sheppard, C.J., Castello, M., Tortarolo, G., Deguchi, T., Koho, S.V., Vicidomini, G., Diaspro, A.: Pixel reassignment in image scanning microscopy: a re-evaluation. Journal of the Optical Society of America A **37**(1), 154–162 (2020)

[17] Kner, P., Chhun, B.B., Griffis, E.R., Winoto, L., Gustafsson, M.G.: Super-resolution video microscopy of live cells by structured illumination. Nature Methods **6**(5), 339–342 (2009)

[18] Reymond, L., Ziegler, J., Knapp, C., Wang, F.-C., Huser, T., Ruprecht, V., Wieser, S.: SIMPLE: Structured illumination based point localization estimator with enhanced precision. Optics Express **27**(17), 24578–24590 (2019)

[19] Reymond, L., Huser, T., Ruprecht, V., Wieser, S.: Modulation-enhanced localization microscopy. Journal of Physics: Photonics **2**(4), 041001 (2020)

[20] Cnossen, J., Hinsdale, T., Thorsen, R.Ø., Siemons, M., Schueder, F., Jungmann, R., Smith, C.S., Rieger, B., Stallinga, S.: Localization microscopy at doubled precision with patterned illumination. Nature Methods **17**(1), 59–63 (2020)

[21] Sun, Y., Yin, L., Cai, M., Wu, H., Hao, X., Kuang, C., Liu, X.: Modulated illumination localization microscopy-enabled sub-10 nm resolution. Journal of Innovative Optical Health Sciences **15**(02), 2230004 (2022)

[22] Kalisvaart, D., Cnossen, J., Hung, S.-T., Stallinga, S., Verhaegen, M., Smith, C.S.: Precision in iterative modulation enhanced single-molecule localization microscopy. Biophysical Journal **121**(12), 2279–2289 (2022)

[23] York, A.G., Chandris, P., Nogare, D.D., Head, J., Wawrzusin, P., Fischer, R.S., Chitnis, A., Shroff, H.: Instant super-resolution imaging in live cells and embryos via analog image processing. Nature Methods **10**(11), 1122–1126 (2013)

[24] Schulz, O., Pieper, C., Clever, M., Pfaff, J., Ruhlandt, A., Kehlenbach, R.H., Wouters, F.S., Großhans, J., Bunt, G., Enderlein, J.: Resolution doubling in fluorescence microscopy with confocal spinning-disk image scanning microscopy. Proceedings of the National Academy of Sciences **110**(52), 21000–21005 (2013)

[25] Tenne, R., Rossman, U., Rephael, B., Israel, Y., Krupinski-Ptaszek, A., Lapkiewicz, R., Silberberg, Y., Oron, D.: Super-resolution enhancement by quantum image scanning microscopy. Nature Photonics **13**(2), 116–122 (2019)

[26] Rossman, U., Tenne, R., Solomon, O., Kaplan-Ashiri, I., Dadosh, T., Eldar, Y.C., Oron, D.: Rapid quantum image scanning microscopy by joint sparse reconstruction. Optica **6**(10), 1290–1296 (2019)

[27] Castello, M., Tortarolo, G., Buttafava, M., Deguchi, T., Villa, F., Koho, S., Pesce, L., Oneto, M., Pelicci, S., Lanzanó, L., *et al.*: A robust and versatile platform for image scanning microscopy enabling super-resolution flim. Nature Methods

16(2), 175–178 (2019)

[28] Buttafava, M., Villa, F., Castello, M., Tortarolo, G., Conca, E., Sanzaro, M., Piazza, S., Bianchini, P., Diaspro, A., Zappa, F., *et al.*: SPAD-based asynchronous-readout array detectors for image-scanning microscopy. Optica **7**(7), 755–765 (2020)

[29] Koho, S.V., Slenders, E., Tortarolo, G., Castello, M., Buttafava, M., Villa, F., Tcarenkova, E., Ameloot, M., Bianchini, P., Sheppard, C.J., *et al.*: Two-photon image-scanning microscopy with SPAD array and blind image reconstruction. Biomedical Optics Express **11**(6), 2905–2924 (2020)

[30] Slenders, E., Perego, E., Buttafava, M., Tortarolo, G., Conca, E., Zappone, S., Pierzynska-Mach, A., Villa, F., Petrini, E.M., Barberis, A., *et al.*: Cooled SPAD array detector for low light-dose fluorescence laser scanning microscopy. Biophysical Reports **1**(2), 100025 (2021)

[31] Stein, S., Thiart, J., Thiele, J.C., Radmacher, N.: TrackNTrace Freeware Package. https://gitlab.gwdg.de/igregor/single-molecule-localization-microscopy-with-image-scanning-microscopy.git (2023)

[32] Stein, S.C., Thiart, J.: TrackNTrace: A simple and extendable open-source framework for developing single-molecule localization and tracking algorithms. Scientific Reports **6**(1), 37947 (2016)

[33] Rieger, B., Stallinga, S.: The lateral and axial localization uncertainty in super-resolution light microscopy. ChemPhysChem **15**(4), 664–670 (2014)

[34] Thiele, J.C., Nevskyi, O., Helmerich, D.A., Sauer, M., Enderlein, J.: Advanced data analysis for fluorescence-lifetime single-molecule localization microscopy. Frontiers in Bioinformatics **1**, 740281 (2021)

[35] Jungmann, R., Avendaño, M.S., Woehrstein, J.B., Dai, M., Shih, W.M., Yin, P.: Multiplexed 3D cellular super-resolution imaging with DNA-PAINT and Exchange-PAINT. Nature Methods **11**(3), 313–318 (2014)

[36] Oleksiievets, N., Sargsyan, Y., Thiele, J.C., Mougios, N., Sograte-Idrissi, S., Nevskyi, O., Gregor, I., Opazo, F., Thoms, S., Enderlein, J., *et al.*: Fluorescence lifetime DNA-PAINT for multiplexed super-resolution imaging of cells. Communications Biology **5**(1), 38 (2022)

[37] Dani, A., Huang, B., Bergan, J., Dulac, C., Zhuang, X.: Superresolution imaging of chemical synapses in the brain. Neuron **68**(5), 843–856 (2010)

[38] Truckenbrodt, S., Maidorn, M., Crzan, D., Wildhagen, H., Kabatas, S., Rizzoli, S.O.: X10 expansion microscopy enables 25-nm resolution on conventional

microscopes. EMBO Reports **19**(9), 45836 (2018)